General Disclaimer

One or more of the Following Statements may affect this Document

- This document has been reproduced from the best copy furnished by the organizational source. It is being released in the interest of making available as much information as possible.

- This document may contain data, which exceeds the sheet parameters. It was furnished in this condition by the organizational source and is the best copy available.

- This document may contain tone-on-tone or color graphs, charts and/or pictures, which have been reproduced in black and white.

- This document is paginated as submitted by the original source.

- Portions of this document are not fully legible due to the historical nature of some of the material. However, it is the best reproduction available from the original submission.

Measurements of Precipitated 1-20 keV Protons and Electrons During a Breakup Aurora*

W. Bernstein, G. T. Inouye, N. L. Sanders and R. L. Wax

*This work was supported by NASA Contract NASW-1474

Space Sciences Laboratory
TRW SYSTEMS
One Space Park
Redondo Beach, California 90278

ABSTRACT

Measurements of precipitating low energy (1-20 keV) protons and electrons during a breakup aurora are described. The observed proton fluxes were as high as 10^8 cm^{-2} sec^{-1} keV^{-1} str^{-1} with an e-fold energy of ~1 keV; the electron fluxes were ~10^8 cm^{-2} sec^{-1} keV^{-1} str^{-1} with a spectral peak in the 2-4 keV region. During the flight, the rocket passed through the poleward boundary of the auroral form. One interpretation of the data suggests that the proton and >2.5 keV electron precipitation boundaries coincided to within a distance of <1 km; the lower energy electron boundary extended several kilometers poleward of the proton boundary. Evidence for non-isotropic proton fluxes is presented.

INTRODUCTION

Only recently have there been direct measurements of energetic protons in the range 0.5 to 20 keV during auroral activity [Chase, 1968; Reasoner, et al. 1968] so that a comparison can be made between electron and proton fluxes at those energies which contain the largest precipitated fluxes. Such a comparison is most valuable in the identification of possible auroral accelerating and modulating mechanisms. Without such comparisons, it is unlikely that the auroral problem will be solved completely. Prior to these direct observations, ground based optical studies of hydrogen Balmer emission [Chamberlain, 1961; Eather, 1967] and satellite survey studies [Johnson, 1967] were the only observations of protons in this energy range. It should be emphasized that most of the existing optical data relate to "proton auroras" and that little work has been done on comparing protons and electrons during active breakup auroras where electrons have been thought to be the dominant precipitating particle. In this paper we will describe observations of both proton and electron flux and energy spectra (0.5-20 keV) which were made during the auroral breakup phase.

INSTRUMENTATION

The proton and electron experiments formed part of a comprehensive Nike-Tomahawk payload which also included a vehicle borne H_β photometer and an experiment to measure AC and DC electric fields in the aurora. The results of these latter experiments will be reported elsewhere.

One characteristic of precipitating hydrogen fluxes is that at altitudes below about 450 km, charge exchange effects begin to occur. Significant

fractions of an incident beam of protons will begin to appear as protons (H^+), hydrogen atoms (H^o) and negative ions (H^-). Below ~250 km the three components should attain their relative equilibrium populations. Allison [1958] has tabulated the pertinent cross sections and equilibrium fractions for protons incident on various gases at various energies. Unfortunately the only existing data for atomic oxygen [Stebbings, 1964], which is the dominant species in the atmosphere above ~200 km, do not include equilibrium fractions; also the work reviewed by Allison does not extend to energies below 3 keV for N_2 or O_2. An extrapolation of the N_2 data to energies less than 1 keV, which is shown in Fig. 1, has been used to correct the observed fluxes of H^o to the flux of protons incident at the top of the atmosphere. It has been assumed that all of the incoming hydrogen flux was originally protons. Because neutral hydrogen is the dominant component in the precipitated beam at altitudes below 250 km, the correction factors that need to be applied to a measured H^o flux are much less significant than those needed for correction of a measured H^+ flux. This is true even if there are small departures from equilibrium because the atmosphere has collapsed and the 250 km altitude no longer corresponds to an equilibrium thickness. Therefore we have chosen to make flux and energy measurements on the H^o component instead of the usual H^+ measurements.

The H^o energy spectrometer has been described previously [Bernstein, et al. 1968]; a simplified schematic of the analyzer is shown in Fig. 2. The electrostatic deflection system removed incident protons with energies <50 keV. During transit of the 2 $\mu g/cm^2$ carbon foil, a fraction (~10%) of the neutral atoms were ionized and their flux and energy spectrum were

determined with the hemispherical electrostatic analyzer and continuous channel multipliers. Laboratory calibrations, which are tabulated by Bernstein, et al, [1968], gave an accurate knowledge of the incoming particle flux and energy. The general characteristics of the instrument are summarized in Table I.

Clearly, the omission of the deflection voltage would have permitted the measurement of total hydrogen and therefore atmospheric corrections would not have been required. However, pin holes are usually present and it is possible that some fraction of the foil could be lost during the flight. Those protons which entered the electrostatic analyzer through regions without foil would have a probability of detection orders of magnitude higher than particles entering through the foil because they would not undergo scattering in the foil. Since the net result of a partial loss of foil without deflection voltage would be a much too high counting rate, we have limited our measurements to the H^o component.

The electron spectrometer consisted of a collimator, and a 90° cylindrical electrostatic analyzer with a continuous channel multiplier detector. The characteristics of this analyzer are also given in Table I. This instrument was programmed to telemeter counting data for a one second period every alternate second.

Both the electron and H^o analyzers were driven by a 4 kV high voltage sweep which allowed a spectrum to be obtained every 10 msec if the counting rates were high enough. The counts were stored in five separate energy channels in the manner described by Bernstein, et al.[1968] the

energy ranges for the five channels are given in Table I. The difference between the H^o and electron channels was due to the correction for the energy lost by the H^o in transit of the foil.

The collimators for both instruments were pointed up along the spin axis of the rocket. Two fluxgate magnetometers measured the orientation of the spin axis with respect to the magnetic field lines. Ground based measurements of 3914Å and 5577Å auroral light emission were provided by the Rocket Range. These photometers had 2° fields of view and were aimed at three successive points along the rocket trajectory. Since the regions where precipitated particles were detected by the rocket were infrequently in the field of view of the photometers, a detailed comparison of particles and light is not too meaningful.

Flight Conditions

The Nike-Tomahawk rocket was launched from Ft. Churchill, Manitoba, Canada into a breakup event at 0001:40 local time (0601:40 UT) on April 25, 1968. The magnetic field was in the recovery phase of a 140γ magnetic bay and was depressed approximately 100γ during the entire rocket flight. About 20 minutes before the flight the main visual breakup had occurred with very bright activity lasting for eight minutes. The aurora began to reform in the north and then at launch brightened considerably and moved southward. The aurora dimmed during its southward movement and, by the time that the rocket flight was terminated, was hardly visible. Figure 3 shows an all-sky camera photograph of the aurora when the rocket

was at a 120 km altitude on the upleg of the flight; the position of the rocket is indicated near the form boundary. It is estimated that there was less than 1/2 db of aurorally enhanced riometer absorption at 30 MHz.

The orientation of the rocket spin axis with respect to the geomagnetic field is shown in Fig. 4. The precession period was rather long, ~4.5 minutes. The axis of precession was inclined 35° to the geomagnetic field; the tip of the rocket traced out a cone inclined 18° to this axis. At 0603:50 the angle between the rocket axis and the field was 27°; at apogee the angle was 56°. The magnetometer indicated that the coning angle during a single spin period was $\leq 1°$.

Experimental Results

Ten second averages of the differential flux of the detected neutral hydrogen atoms in each of the five energy channels are shown in Fig. 5. At 0604:20 one of the two telemetry transmitters failed with the consequent loss of some channels of both the H^o and electron spectrometers. The H^o data have been corrected for solid angle, detector efficiency, variable energy resolution, and for the fraction of time that a given channel was counting. The spectra shown in Fig. 6 are typical of those obtained during the flight. In these spectra, the data of Fig. 5 have been further corrected by the equilibrium fractions, given in Fig. 1, to obtain the total hydrogen precipitation. As can be seen in Fig. 6A, the differential spectrum fits well to a power law ($E^{-n}_{(keV)}$) dependence with n = 3.2. Alternatively, Fig. 6B shows that the spectrum is also consistent with an exponential dependence, and shows an e-fold energy of ~1 keV. The ten

second averages of the hydrogen flux and e-folding energy are shown in Figs. 7A and 7B, respectively, during the period when complete five channel data were available. There was no evidence for a large change in either the average flux or energy spectrum during this period.

The temporal dependence of the electron fluxes observed in the five energy channels, after correction for solid angle, resolution, and channel counting time is shown in Fig. 8. The spectrum was of a peaked nature throughout the reported time period. Initially the peak flux was observed in Channel 2 (1.1 - 2.5 keV); after 0603:40 UT, the flux in this channel decreased and the peak flux was observed in Channel 3 (2.5 - 6 keV). At this time, no change of a similar magnitude was observed in either the hydrogen flux or energy spectrum.

Figure 9 shows the temporal behavior of the λ3914Å and λ5577Å light intensity measured by the ground based photometers. The general temporal behavior of these measurements was in good agreement with that of the electrons and protons, and further indicated that the auroral activity decreased rapidly at ~0605:25 UT.

Figure 10 shows the 1 sec averages of the counting rates observed in the 1.5 - 3 keV and 7 - 11 keV hydrogen channels and the 2.5 - 6 keV electron channel on an expanded time scale during the period when auroral activity ceased. The counting rate was such that times of less than one second would not be statistically significant. There did not appear to be a difference of greater than one second in either the decay time (11 sec) or the time of initiation of the decay (0605:27 UT) between the two

proton energy channels. The decay time of the 2.5 - 5 keV electron channel appeared to be ~8 sec and the initiation was about three seconds later than that for the protons. The behavior of the 0.5 - 1.1 keV electron channel was significantly different. It showed an increase in flux prior to the initiation of the proton decay, and the flux remained at a relatively high level for almost another minute with an ~10 sec oscillation period before dropping abruptly at 0606:20 UT.

Discussion

The observed high intensity (10^8 cm^{-2} sec^{-1} str^{-1} keV^{-1}) and small e-fold energy (~1 keV) of precipitated total hydrogen flux appears to be in good agreement with the data reported by Chase [1968] and by Reasoner, et al. [1968] for post breakup auroras. These results differ considerably from the quiet proton arc data reported by Whalen, et al. [1967] where fluxes 10^7 cm^{-2} sec^{-1} str^{-1} keV^{-1} and e-fold energies of ~12 keV were observed. However in that experiment, the lowest proton energy measured was ~30 keV. It is therefore uncertain whether the discrepanices correspond to a difference in the precipitation phenomenon, or whether they can be attributed entirely to the presence of a large flux of low energy protons which would not be detected by Whalen's instruments. The peaked electron spectra are consistent with those previously reported by Evans [1967] and by Albert [1967].

The present observations indicate that a significant fraction (~0.5) of the total precipitated energy flux was deposited by protons. The time dependence of the electron and total hydrogen components of the precipitated

energy flux is shown in Fig. 11 for the time period during which complete spectral data was recorded. The intensity of the 3914Å radiation leads to an estimate of the total energy dumped into the aurora (~10 ergs/cm^2) which is in reasonable agreement with the energy observed in the particles.

Except for measurements performed during quiet proton arcs, all previous measurements indicate that the ratio of the proton precipitated energy flux to that of the electrons is typically $\leq$0.1 [Chamberlain, 1961]. These observations have led to the conclusion that proton precipitation is usually an unimportant factor in such auroral phenomena. The large and comparable fraction assigned to protons in the present flight may be due to the fact that the rocket was located near the edge of the auroral form. Proton spreading resulting from charge exchange may lead to a significant change in the ratio of the observed precipitated energy fluxes of the two components as one moves across the precipitation zone. However, the relative constancy in the ratio over the 89 sec observation period can indicate that the total proton energy deposition was indeed comparable to the total electron energy deposition.

With the exception of the lowest energy electron channel, all of the various measurements showed the cessation of precipitation beginning at approximately 0605:27. Although it is possible to derive either spatial or temporal explanations for this event, the present experimental data appears to be more consistent with spatial effects. Together with other requirements, a temporal cause must take account of the lack of any dispersion >1 sec in the arrival times of the protons in the two energy channels and the persistence of electron precipitation after the initiation of

proton cessation. The proton arrival time dispersion would locate the proton precipitation control region at a distance of <1000 km above the rocket if it is assumed that all proton precipitation ceased at the same time.

The spatial explanation leads to several physical requirements for the proton precipitation process. During the observed precipitation decay time (11 sec) the total distance traversed by the rocket was ~11 km; the north-south distance was only 1.5 km. This fact implies that the proton flux fell off far more rapidly with north-south distance than suggested by Davidson [1965] in his calculations of the lateral spreading of precipitated protons based upon two assumed pitch angle distributions. Two possible explanations for this discrepancy are (1) the precipitated proton pitch angle distribution was more sharply peaked along the field lines than both assumed distributions, and/or (2) the temperature of the upper atmosphere above Ft. Churchill was less than that assumed by Davidson. If the temperature were responsible, an altitude of 200 km could have corresponded to Davidson's 300 km altitude with a consequent decrease in the predicted charge exchange spreading of precipitated protons. We have no data on the local ionospheric temperatures during the flight. There was, however, an indication that the pitch angle distribution was not isotropic.

Because the instrument apertures were aligned parallel to the rocket spin axis, a near isotropic flux would not be expected to produce a spin modulation of the counting rates. In order to search for such a modulation indicative of a non-isotropic precipitation and also for other periodic variations in the counting rate data, the analog telemetry signals of the

two hydrogen channels available for the whole flight were digitized. The auto correlation, cross correlation, coherence functions, single power spe.tra and crossed spectra were computed. The crossed spectra, both of the individual power spectra, and the coherence function showed the most pronounced peak was at 0.68 Hz. This agrees to within 0.01 Hz of the spin frequency derived from the on-board magnetometer data. Because of the vehicle precession, the angle between the spin axis and the geomagnetic field was ∿20° at 0602:50 UT and increased to 56° at apogee when precipitation ceased. However, the counting rates were too low to permit a fine enough time scale to identify a dependence in the degree of spin modulation on the vehicle precession angle. The existence of spin modulation indicates that the precipitation was not isotropic over angles 20-56°. The alternate second sampling of the electron distribution precluded any possibility of a similar analysis of the electron data; therefore we have no information with respect to the degree of electron isotropy during the flight.

The electron behavior during cessation at 0605:27 UT showed different patterns for the two electron energy channels. The behavior of the higher energy (2.5 - 6 keV) channel was similar to that observed for protons and so was at least consistent with a spatial cause for the cessation. The 0.5 - 1.1 keV channel, however, showed an enhancement prior to 0605:25 UT followed by a 10 second period oscillation before an abrupt decay some 43 seconds later. This pattern would indicate that temporal effects must have been present in addition to spatial effects. The general pattern supports the conclusion that proton and electron precipitation are

intimately related during the breakup phase and that the observed patterns are not the result of the fortuitous time coincidence of two independent precipitation processes.

CONCLUSIONS

The following conclusions can be drawn about the aurora into which the present flight was launched.

1. The fluxes of precipitated electrons and protons appear to be directly correlated on a long (minute) time scale.

2. The energy flux precipitated by protons was comparable to that precipitated by electrons. The total precipitated energy flux in the range 1-10 keV easily accounted for the observed optical emissions.

3. Short time fluctuations (~1 sec) in the flux and energy spectrum of protons and electrons appeared to be unrelated.

4. A spatial explanation for the cessations of precipitation suggests that the poleward boundary of the proton precipitation region coincided within a distance of <1 km with the poleward boundary of >2.5 keV electron precipitation. Very low energy, <2.5 keV, electron precipitation extended several kilometers further poleward than the proton boundary.

5. The proton pitch angle distribution was not isotropic.

ACKNOWLEDGMENTS

We wish to thank E. Offer, W. Simpson and R. Alexander for their help during this program. W. Conner and R. Schamaley of the NASA Sounding Branch provided the telemetry system. We wish to thank other members of the Sounding Rocket Branch and Churchill Research Range personnel for their support during flight.

REFERENCES

Albert, R. D., Energy and flux variations of nearly monoenergetic auroral electrons, J. Geophys. Res., 72, 5811, 1967.

Allison, S. K., Experimental results on charge changing collisions of hydrogen and helium atoms and ions at kinetic energies above 0.2 keV, Rev. Mod. Phys., 30, 1137, 1958.

Bernstein, W., R. L. Wax, G. T. Inouye, and N. L. Sanders, An energy spectrometer for energetic (1-20 keV) neutral hydrogen atoms, presented at the COSPAR Symposium held in Tokyo, May 1968.

Chamberlain, J. W., Physics of the Aurora and Airglow, Academic Press, Inc., New York, 1961.

Chase, L. M., Spectral measurements of auroral zone particles, J. Geophys. Res., 73, 3469, 1968.

Davidson, G. T., Expected spatial distribution of low energy protons precipitated in the auroral zone, J. Geophys. Res., 70, 1061, 1965.

Eather, R. H., Auroral proton precipitation and hydrogen emission, Rev. of Geophysics, 5, 207, 1967.

Evans, D. S., A 10 cps periodicity in the precipitation of auroral-zone electrons, J. Geophys. Res., 72, 5811, 1967.

Johnson, R. G., R. E. Meyerott, and J. E. Evans, Coordinated satellite, ground-based and aircraft-based measurements on auroras, in Aurora and Airglow, edited by B. M. McCormac, Reinhold Publishing Corp., New York, 1967.

Reasoner, D. L., R. H. Eather, and B. J. O'Brien, Detection of alpha particles in auroral phenomena, J. Geophys. Res., 73, 4185, 1968.

Stebbings, R. F., A. C. H. Smith, and H. Ehrhardt, Charge transfer between oxygen atoms and O^+ and H^+ ions, J. Geophys. Res., 11, 2349, 1964.

Whalen, B. A., I. B. McDiaimid, and E. E. Budzinski, Rocket measurements in proton aurora, Can. J. Phys., 45, 3247, 1967.

Table 1

	H^o Spectrometer	Electron Spectrometer
Energy Channels (keV)	0.6 - 1.5	0.5 - 1.1
	1.5 - 3.4	1.1 - 2.5
	3.4 - 7.0	2.5 - 6.0
	7.0 - 11.5	6.0 - 10.5
	11.5 - 22.0	10.5 - 21.0
Geometrical Factor (cm^2 str)	4.3×10^{-2}	1.3×10^{-3}
Resolution for an incident isotropic flux (FWHM)	19%	12%
Look Angle	Along spin axis	Along spin axis
Analyzer factor	5 keV/kV	5 keV/kV

FIGURE CAPTIONS

Figure 1. An extrapolation (solid line) of data given by Allison [1958] (dots) for the equilibrium fraction of neutral hydrogen in a hydrogen beam passing through nitrogen gas.

Figure 2. Schematic diagram of the neutral hydrogen energy spectrometer.

Figure 3. All-sky camera picture 70 sec after launch at 0602:55 UT. The circle indicates the approximate position of the rocket. North is at the top of the picture.

Figure 4. Orientation of the rocket spin axis with respect to the geomagnetic field during the flight.

Figure 5. 10 sec averages of the neutral hydrogen differential flux. Telemetry failure caused data loss after 0604:20.

Figure 6. Total hydrogen differential energy spectra. (A) shows fit to a E^{-n} spectrum and (B) shows fit to a $F_o e^{-E/E_o}$ spectrum.

Figure 7. 10 sec average of (A) the differential flux, F_o, and (B) the e-fold energy, E_o, of total hydrogen for an energy spectrum of the form $F_o e^{-E/E_o}$ during the period when full data were available.

Figure 8. 10 sec averages of the electron differential flux.

Figure 9. Time history of the 3914Å and 5577Å light intensity for the flight.

Figure 10. 1 sec average fluxes of hydrogen and electron fluxes at the time when the rocket passed through the poleward boundary of the auroral form.

Figure 11. 10 sec average of the total energy flux of the electron and total hydrogen precipitation.

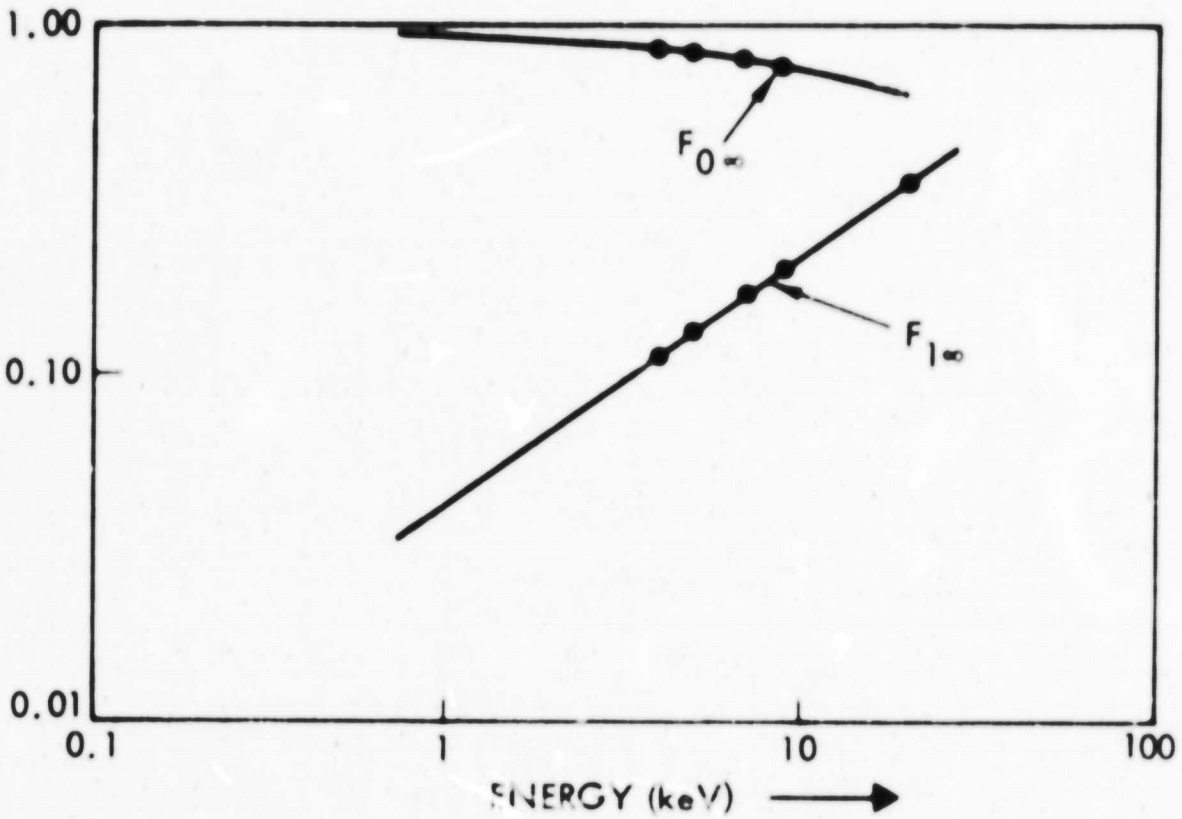
1.00
0.10
0.01
EQ. FRACTIONS
$F_{0\infty}$
$F_{1\infty}$
0.1
1
10
100
ENERGY (keV)

Figure 1

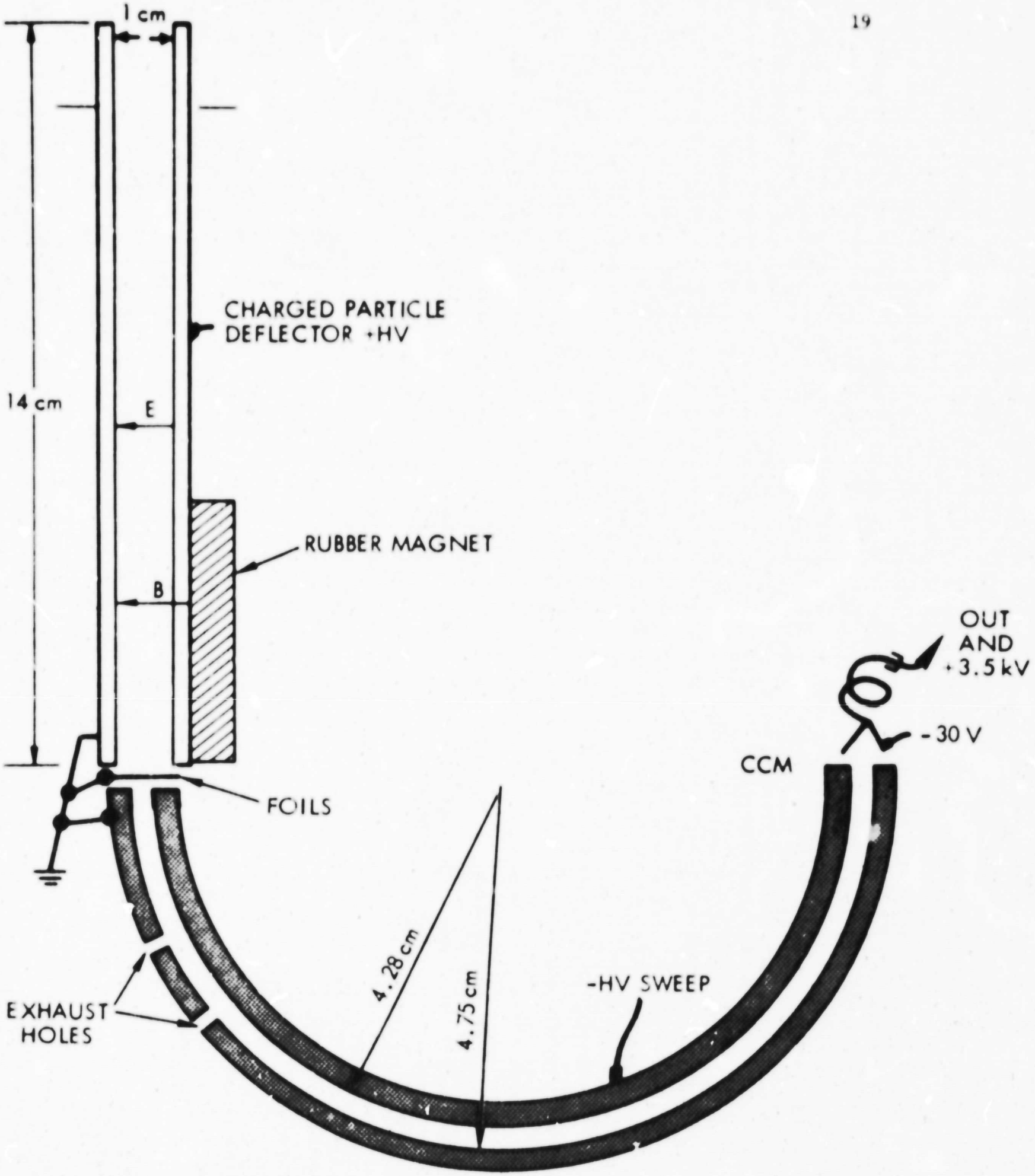
1 cm
CHARGED PARTICLE
DEFLECTOR +HV
14 cm
E
RUBBER MAGNET
B
OUT
AND
+3.5kV
-30 V
CCM
FOILS
4.28cm
4.75cm
-HV SWEEP
EXHAUST
HOLES

Figure 2

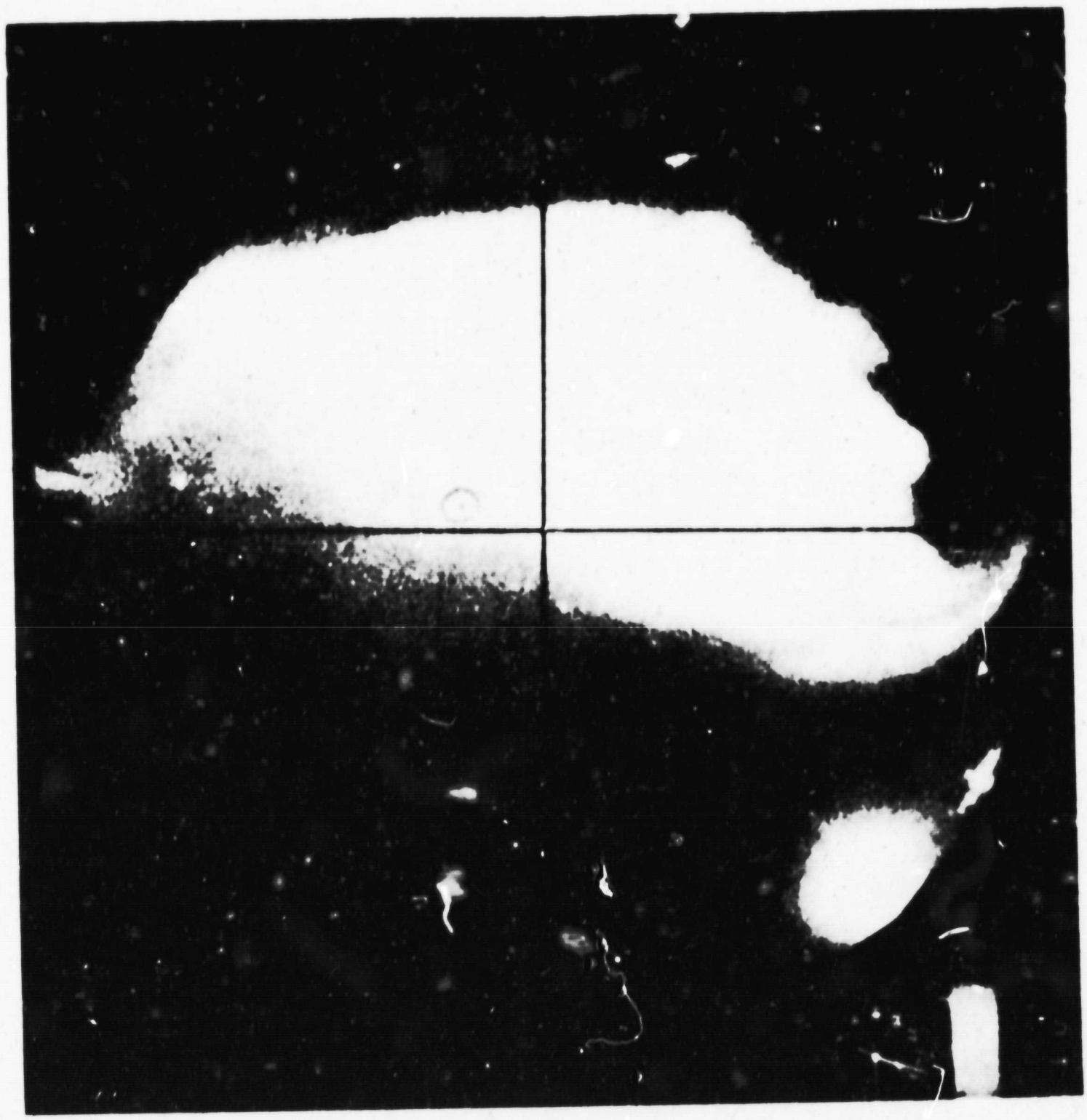

Figure 3

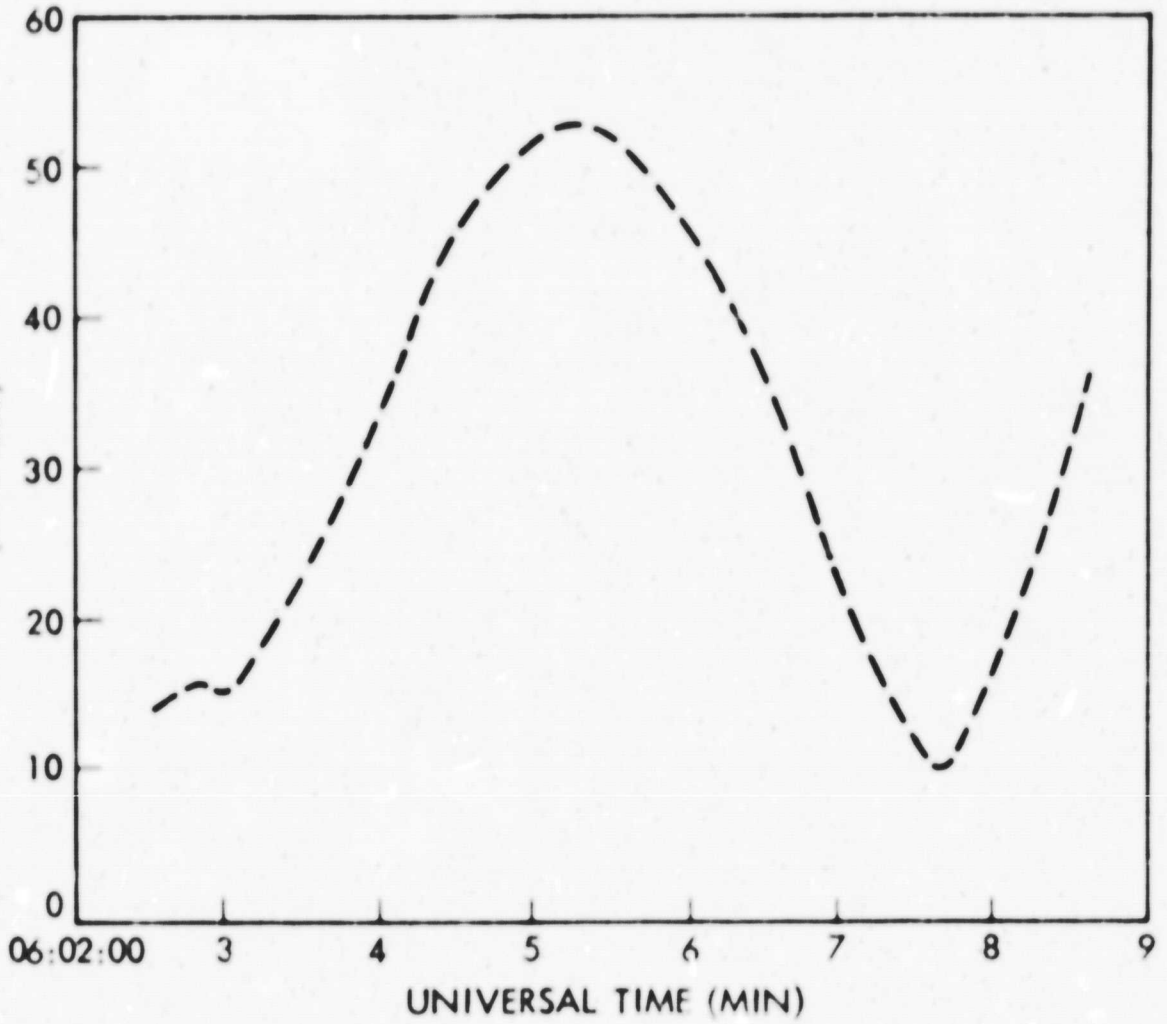
60
50
40
30
20
10
0
θ (DEGREES)
06:02:00
3
4
5
6
7
8
9
UNIVERSAL TIME (MIN)

Figure 4

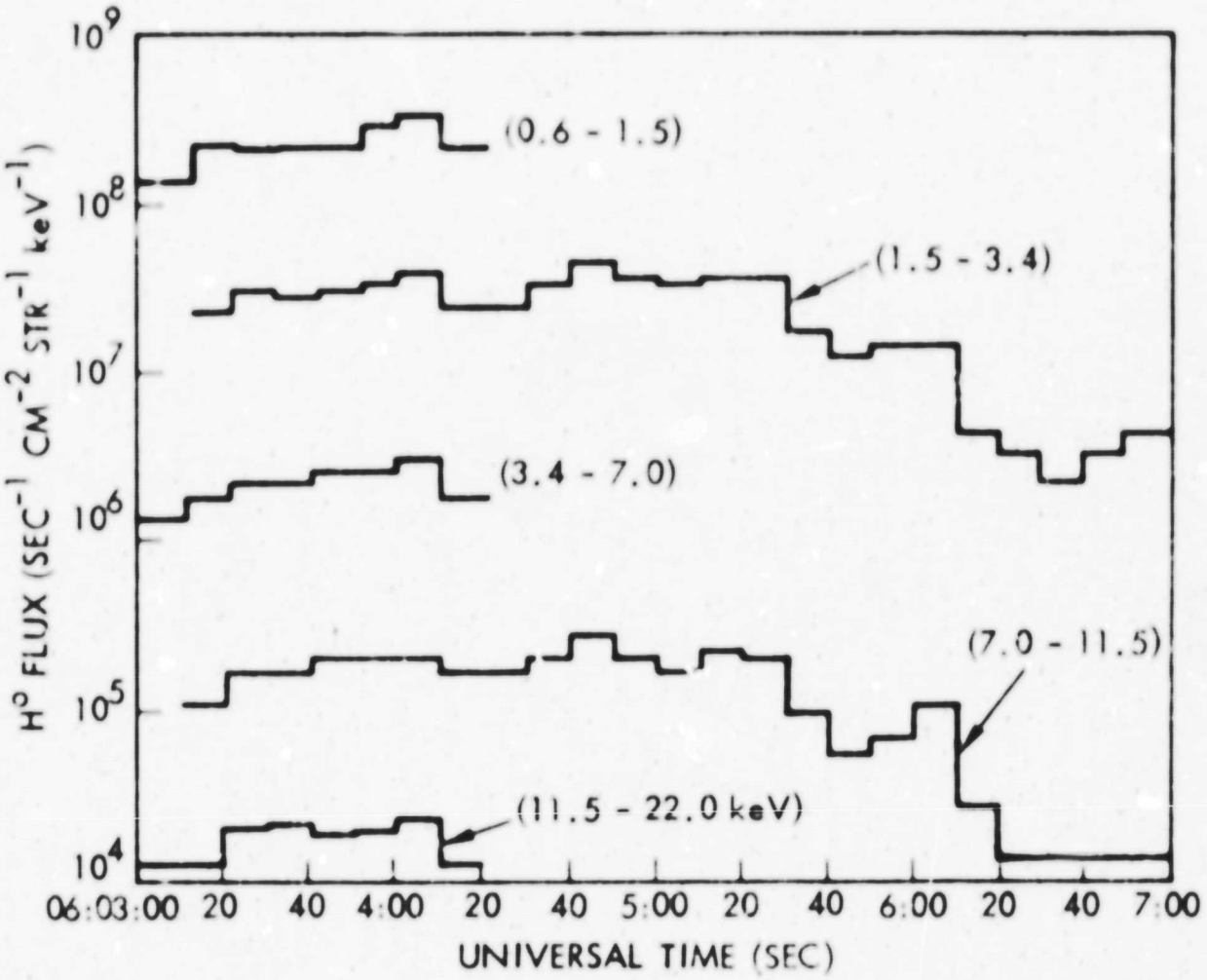
10^9
10^8
10^7
10^6
10^5
10^4
H^o FLUX (SEC^{-1} CM^{-2} STR^{-1} keV^{-1})
(0.6 - 1.5)
(1.5 - 3.4)
(3.4 - 7.0)
(7.0 - 11.5)
(11.5 - 22.0 keV)
06:03:00 20 40 4:00 20 40 5:00 20 40 6:00 20 40 7:00
UNIVERSAL TIME (SEC)

Figure 5

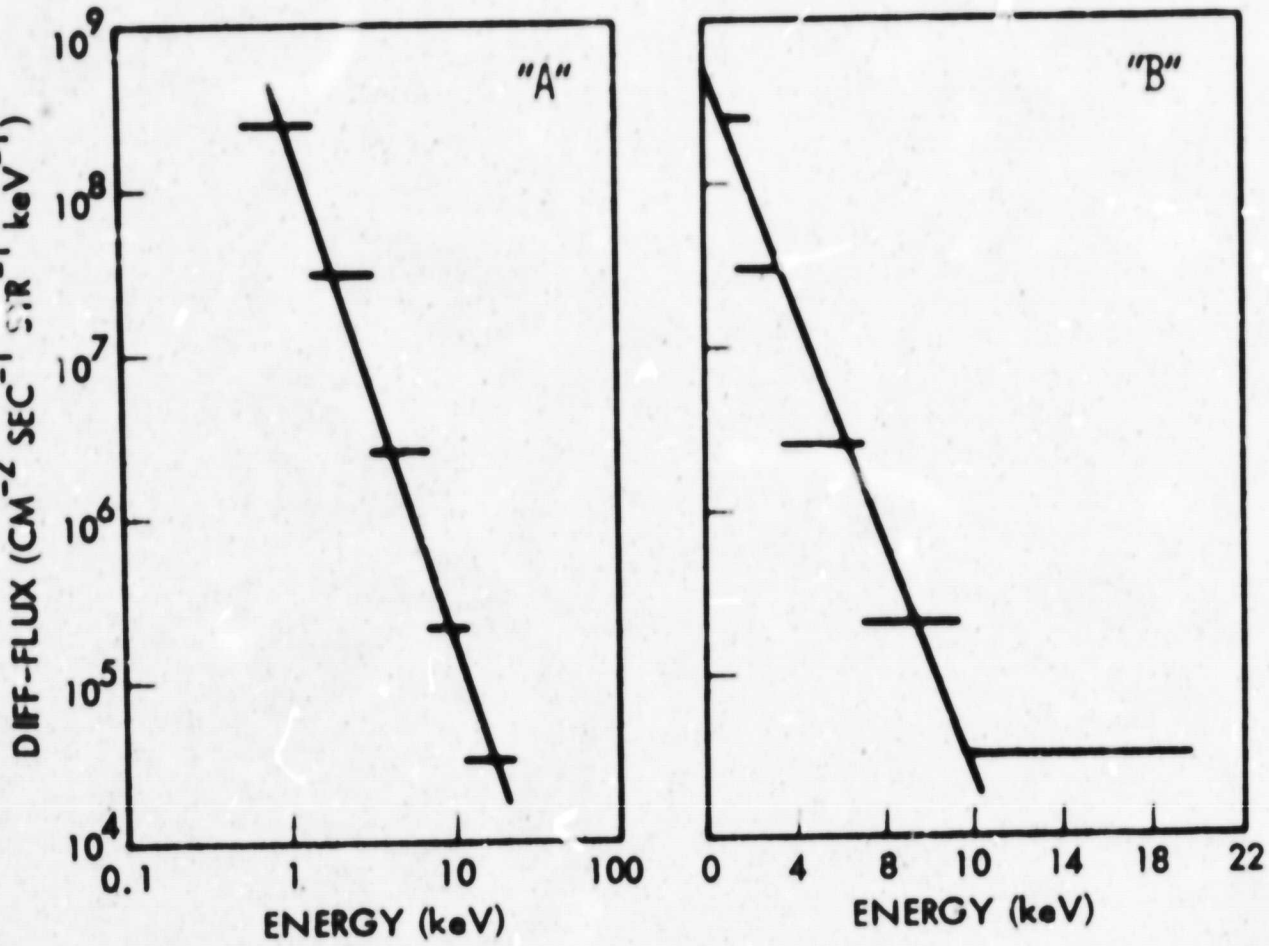
"A"
"B"
DIFF-FLUX (CM^{-2} SEC^{-1} SR^{-1} keV^{-1})
10^9
10^8
10^7
10^6
10^5
10^4
0.1
1
10
100
0
4
8
10
14
18
22
ENERGY (keV)
ENERGY (keV)

Figure 6

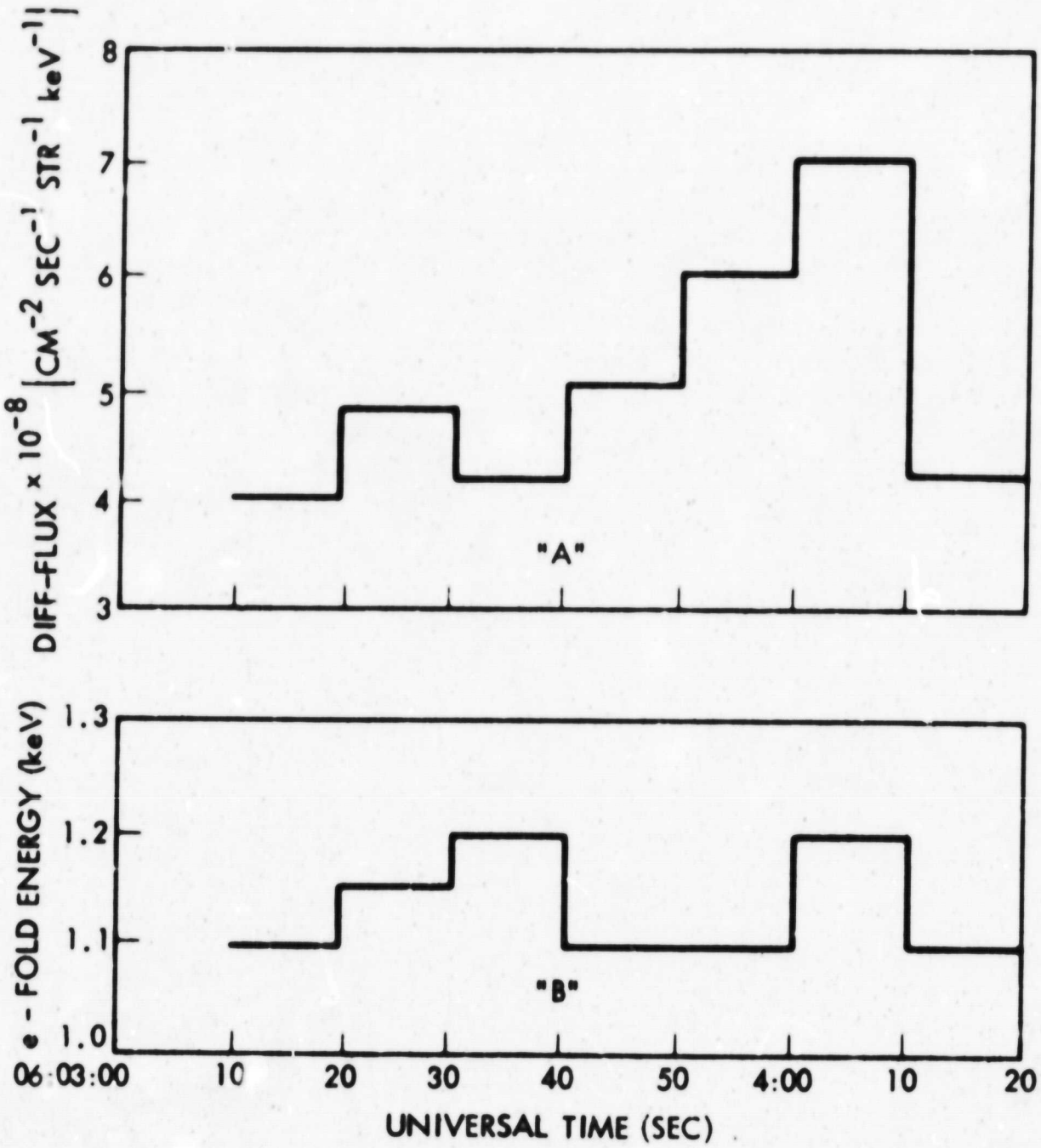
DIFF-FLUX × 10^-8 |CM^-2 SEC^-1 STR^-1 keV^-1|
8
7
6
5
4
3
"A"
e - FOLD ENERGY (keV)
1.3
1.2
1.1
1.0
"B"
06 03:00
10
20
30
40
50
4:00
10
20
UNIVERSAL TIME (SEC)

Figure 7

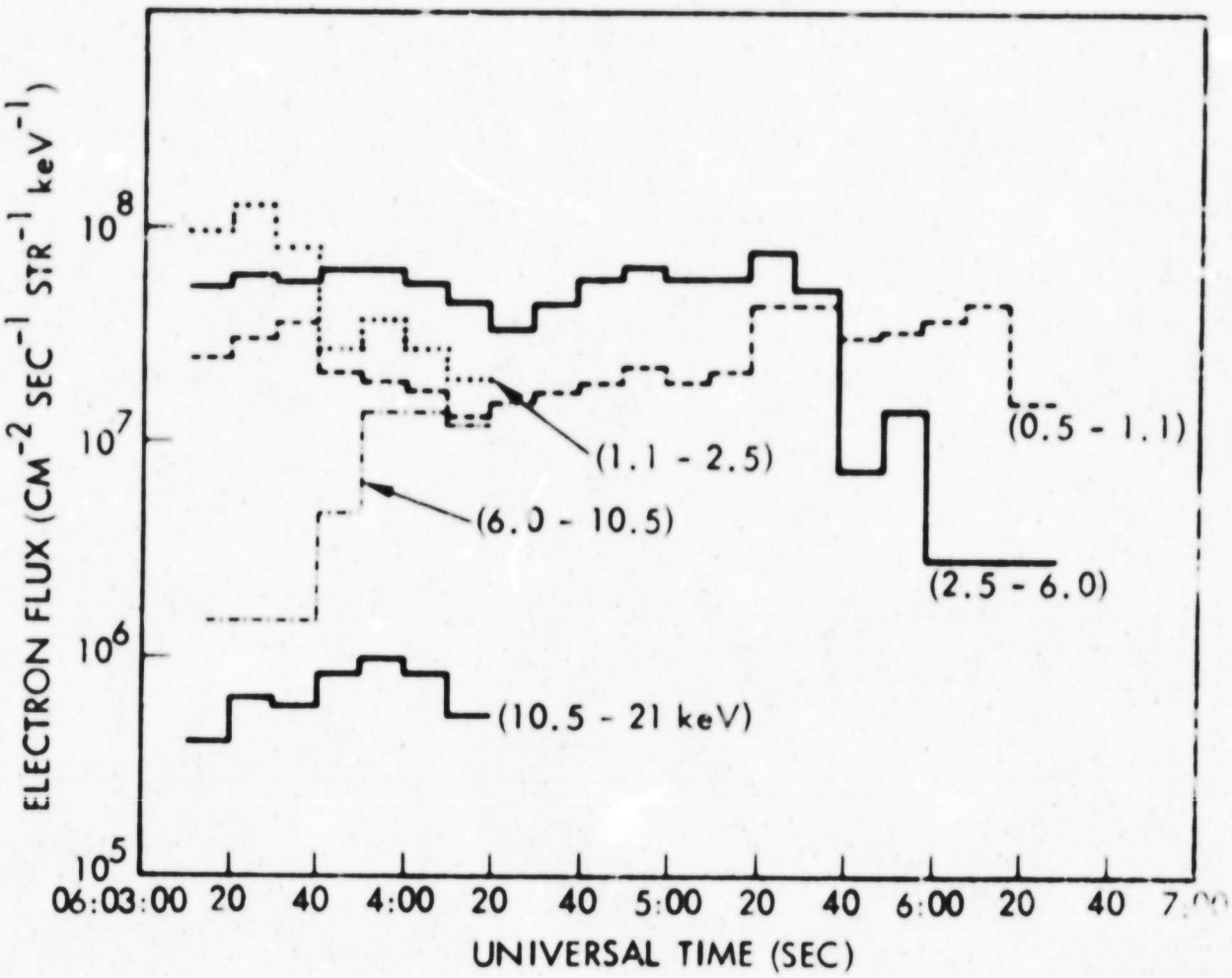
ELECTRON FLUX (CM^{-2} SEC^{-1} STR^{-1} keV^{-1})
10^8
10^7
10^6
10^5
(0.5 - 1.1)
(1.1 - 2.5)
(2.5 - 6.0)
(6.0 - 10.5)
(10.5 - 21 keV)
06:03:00 20 40 4:00 20 40 5:00 20 40 6:00 20 40 7:00
UNIVERSAL TIME (SEC)

Figure 8

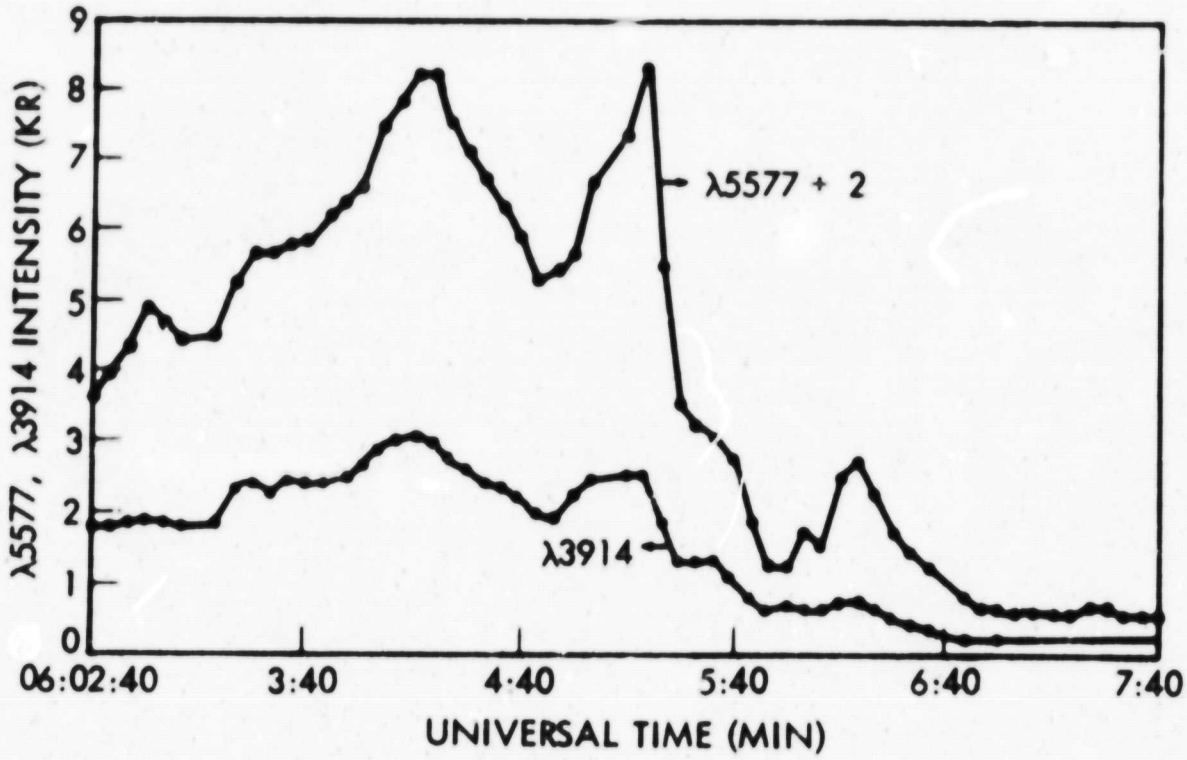
λ5577 + 2
λ3914
λ5577, λ3914 INTENSITY (KR)
0
1
2
3
4
5
6
7
8
9
06:02:40
3:40
4:40
5:40
6:40
7:40
UNIVERSAL TIME (MIN)

Figure 9

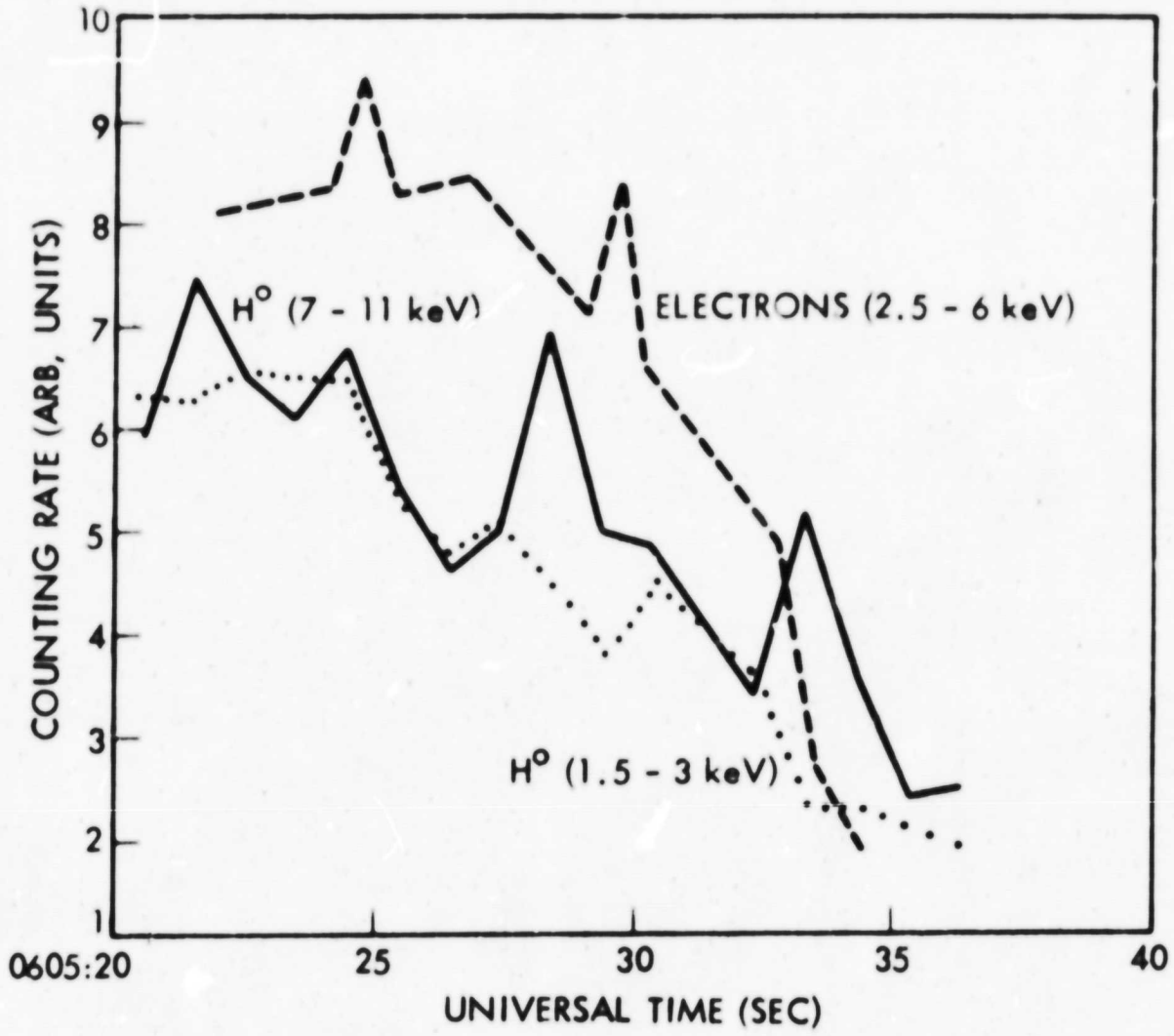
10
9
8
7
6
5
4
3
2
1
COUNTING RATE (ARB, UNITS)
H° (7 - 11 keV)
ELECTRONS (2.5 - 6 keV)
H° (1.5 - 3 keV)
0605:20
25
30
35
40
UNIVERSAL TIME (SEC)

Figure 10

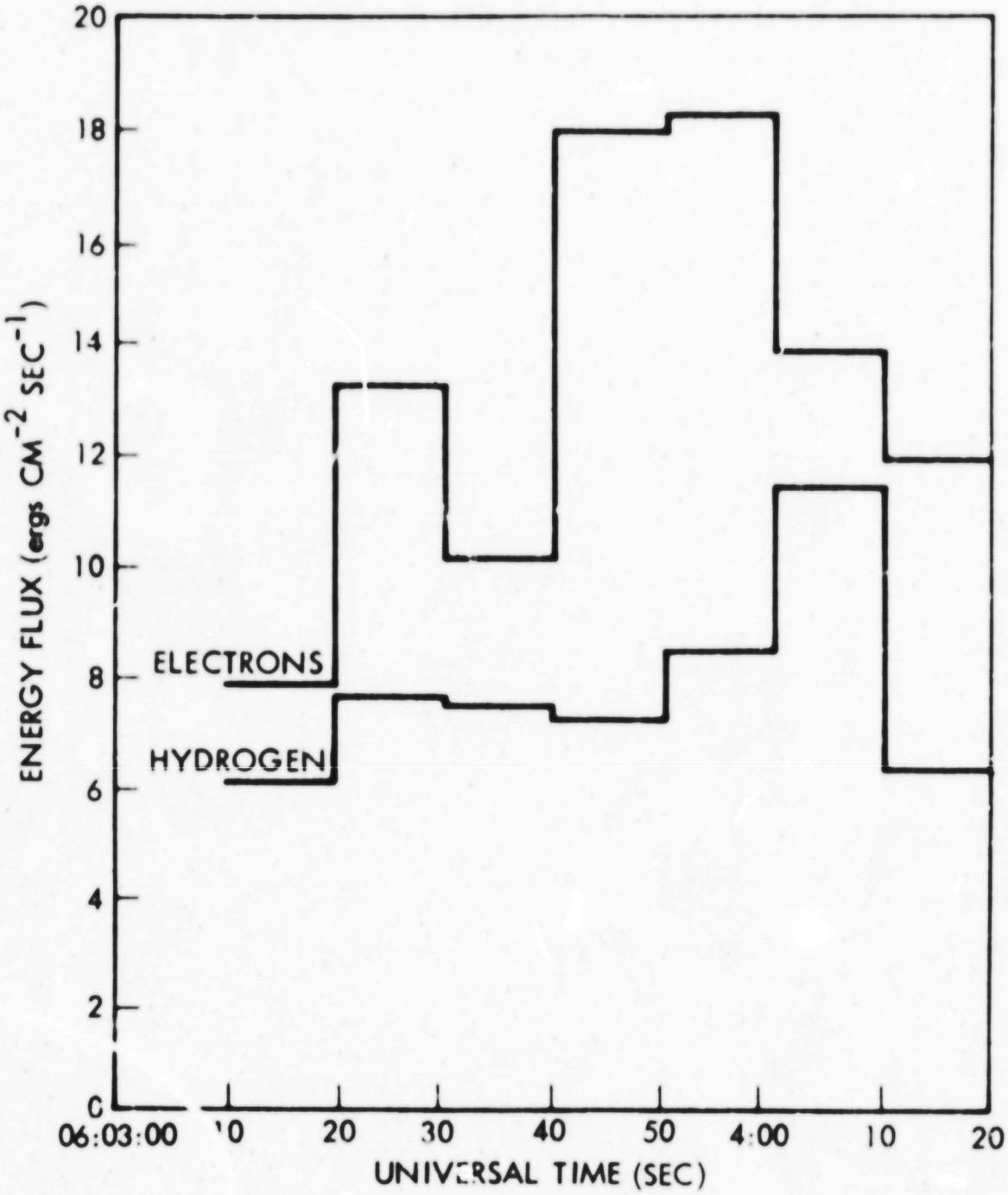
ENERGY FLUX (ergs CM^{-2} SEC^{-1})
20
18
16
14
12
10
8
6
4
2
0
ELECTRONS
HYDROGEN
06:03:00
10
20
30
40
50
4:00
10
20
UNIVERSAL TIME (SEC)

Figure 11